Griffiths phase–like behavior in nearly half-metallic CoFeVAl: Theory and experiment

Barnabha Bandyopadhyay,[1] Jadupati Nag,[1,2] Sabyasachi Paul,[1] M. K. Chattopadhyay,[3,4] Archana Lakhani,[5] Aftab Alam,[1,*] and K. G. Suresh[1,†]

[1]*Department of Physics, Indian Institute of Technology Bombay, Mumbai 400076, India*
[2]*Materials Research Institute, Millennium Sciences Complex, Pennsylvania State University, University Park, Pennsylvania 16802, USA*
[3]*Free Electron Laser Utilization Laboratory, Raja Ramanna Centre for Advanced Technology, Indore 452 013, India*
[4]*Homi Bhabha National Institute, Training School Complex, Anushakti Nagar, Mumbai 400094, India*
[5]*UGC-DAE Consortium for Scientific Research, University Campus, Khandwa Road, Indore 452001, India*

(Received 3 February 2024; accepted 11 March 2024; published 25 March 2024)

We report a combined theoretical and experimental study of the quaternary Heusler alloy CoFeVAl hosting various interesting electronic/magnetic features including an extended Griffiths phase–like behavior. The room temperature x-ray diffraction pattern confirms a cubic structure (space group No. 216) with a B2 disorder between V and Al atoms. The dc magnetization measurements indicate a ferromagnetic-like behavior with a magnetic transition temperature (T_C) ∼50 K. Above T_C an unusual magnetic phase (extended Griffiths like) is observed which is carefully analyzed from the dc and ac magnetic susceptibility data. Longitudinal resistivity data confirm a metallic-like behavior with a negative nonsaturating magnetoresistance in the magnetically ordered region. The anomalous Hall effect mediated by a non-negligible intrinsic mechanism is found in the total Hall resistivity whereas negative slope in the ordinary Hall resistivity indicates the electron-mediated conduction in CoFeVAl. First-principles calculated results corroborate well with the experimentally observed crystal structure and nearly half-metallic ferromagnetic (FM) behavior. A high spin polarization (∼86%) is observed in the FM ground state. Inclusion of B2 disorder retains the nearly half-metallic behavior of CoFeVAl. Such combined studies for the discovery of new quantum materials are the backbone of a future path toward the spintronic-based device applications.

DOI: 10.1103/PhysRevB.109.094433

I. INTRODUCTION

Heusler alloys have attracted a great deal of attention due to various interesting magnetic phenomena exhibited by them, such as itinerant and localized magnetism, ferro-, antiferro-, and ferrimagnetism, and Pauli paramagnetism. Exotic physical properties and a high degree of structural stability have made them potential candidates for various applications such as spintronics, magneto-optics, and caloritronics [1,2]. Half-metallic or nearly half-metallic ferromagnets are observed to play a key role in spintronic-based applications because of their high spin polarization [3,4]. Among the different Heusler alloys, equiatomic quaternary Heusler alloys (EQHAs) are identified as $XX'YZ$ and have been reported to host several interesting magnetic and magnetotransport properties such as half-metallic ferromagnetism [5] and spin gapless semiconductor [6], bipolar magnetic semiconductor [7], and spin semimetallic behavior [8]. The contribution of three different magnetic elements to the total magnetization in EQHAs often leads to numerous interesting magnetic properties. At the same time, the high degree of similarity in the chemical properties (namely, electronegativity) of the constituent elements often leads to the formation of antisite disorder, which in turn has significant impact on the magnetic and magnetotransport properties [9–11].

CoFeVSb is reported to be a spin semimetal with potential spin valve features. The latter originates from the antisite-disorder-induced antiparallel magnetic alignment of Co and Fe atoms in the V sites within the overall ferromagnetic matrix [12]. In this system, the electronegativity of Sb (2.05) is a little higher than that of Co (1.88), Fe (1.83), and V (1.63). Because of this, there is no disorder in the Sb sites, while all the other three atoms occupy each other's sites. This turns out to be responsible for the coexistence of competing magnetic phases and the spin valve feature. Since Heusler alloys are very much prone to this kind of antisite disorder, which plays a major role in determining various novel properties, we have prepared another EQHA, namely, CoFeVAl, where we have replaced Sb by Al completely. Aluminium has an electronegativity of 1.61, which is very close to that of other transition metals. Hence we expect that Al will also take part in the antisite disorder and facilitate distinct electronic/magnetic properties.

In this paper, we report a combined theoretical and experimental study of CoFeVAl, which shows a nearly half-metallic feature with several interesting structural, magnetic, and transport properties. CoFeVAl is found to crystallize in prototype LiMgPdSn structure with small antisite disorder (between V and Al), as revealed by the room temperature (RT) x-ray diffraction (XRD) measurement. The dc magnetization measurements indicate nearly saturated ferromagnetic behavior at

*aftab@iitb.ac.in
†suresh@phy.iitb.ac.in

very low temperatures with a magnetic transition at around 50 K. A careful analysis of dc and ac magnetic susceptibility shows an unusual magnetic phase between the fully ordered and fully disordered phases, namely an extended Griffiths-like phase. Longitudinal resistivity measurement indicates the metallic behavior. Magnetoresistance measurement shows negative MR up to the magnetic transition temperature, reconfirming the ferromagnetic nature of CoFeVAl. Hall measurements show the existence of nonzero anomalous Hall effect (AHE) in the magnetically ordered phase. For deeper insights, first-principles calculations are performed in both ordered and B2 disordered phases of CoFeVAl, which reconfirm the nearly half-metallic behavior with a high spin polarization (∼86%). Interestingly, the spin polarization remains robust in the B2 disordered phase. Thus, the substitution of Sb by Al in CoFeVSb not only reduces the long-range magnetic ordering, but also facilitates several interesting magnetic properties above the transition temperature, making CoFeVAl a promising candidate in the field of magnetic functional materials.

II. EXPERIMENTAL AND THEORETICAL DETAILS

A. Experimental details

A polycrystalline sample of CoFeVAl was prepared using the arc-melting method in a high-purity argon atmosphere. The constituting elements of 99.99% were taken in the exact stoichiometric ratio for the melting. To ensure the homogeneity, the sample was melted 4–5 times by flipping. The as-cast ingot was then annealed for 10 days at 900 °C and then quenched in an ice-water bath in order to obtain the desired phase. XRD pattern was recorded using Cu-Kα with the help of a Panalytical X′Pert diffractometer. Crystal structure analysis was carried out using the Rietveld refinement method implemented in the FullProf Suite software [13]. To investigate the atomic composition and homogeneity of the samples, energy-dispersive x-ray spectroscopy (EDS) was also performed using the JEOL JSM-7600F field electron gun-scanning electron microscope (FEG-SEM) system. The dc and ac magnetization (M) measurements were performed by varying both temperature (T) and magnetic field (H) using a superconducting quantum interference device–based vibrating sample magnetometer (SVSM; Quantum Design, USA). The M-T measurements were performed in the zero-field-cooled (ZFC) as well as in the field-cooled-cooling (FCC) modes. Magnetotransport measurements were performed up to a magnetic field of 90 kOe in a physical property measurement system (PPMS; Quantum Design, USA) at UGC-DAE Consortium on Scientific Research, Indore, India.

B. Computational details

To investigate the structural, magnetic, and transport properties, first-principles calculations were performed using density functional theory (DFT) [14] implemented in the Vienna *ab initio* Simulation Package (VASP) [15–17] in the projected augmented wave (PAW) basis [18]. The exchange correlation potential of Perdue, Burke, and Ernzerhof (PBE) [19] was used within the generalized gradient approximation (GGA) scheme. Brillouin zone integration was performed using the tetrahedron method in an optimized $20 \times 20 \times 20$ k mesh. The optimized plane wave energy cutoff of 350 eV was used for all the calculations. The convergence criteria of 10^{-6} eV was used for all the structural optimization calculations. To simulate the B2-type antisite disorder, we have generated a special quasirandom structure (SQS) [20] using the MCSQS code implemented in the Alloy Theoretic Automated Toolkit (ATAT) [21] package. SQS gives a reasonably approximate structure incorporating the random correlations in the disordered phase. We have considered the random pair correlations up to the fifth nearest neighbors and random triplet correlation up to the third nearest neighbor while generating the SQS structure.

III. EXPERIMENTAL RESULTS

A. Crystal structure (x-ray diffraction)

CoFeVAl crystallizes in the LiMgPdSn-type structure (space group No. 216), which is considered as the prototype for EQHA. This type of structure can be understood as the four fcc sublattices, that are interpenetrated along the body diagonal direction, occupying the Wyckoff positions $4a(0, 0, 0)$, $4b(0.5, 0.5, 0.5)$, $4c(0.25, 0.25, 0.25)$, and $4d(0.75, 0.75, 0.75)$. If we consider any of the four elements to be fixed at a particular atomic site, then depending on the relative site occupancies of the other three elements, there are three possible nondegenerate atomic configurations that exist in EQHA. These configurations (considering the Z element to be fixed at 4a) are shown here [12]:

Type I: X at $4d$, X' at $4b$, and Y at $4c$.
Type II: X at $4d$, X' at $4c$, and Y at $4b$.
Type III: X at $4b$, X' at $4d$, and Y at $4c$.

Primitive unit cells of the three aforementioned atomic configurations are shown in Fig. 1(a). From the Rietveld refinement method, it is found that CoFeVAl crystallizes in the type II configuration with a specific antisite disorder, with the lattice constant $a_0 = 5.78$ Å. Figure 1(b) shows the room temperature XRD pattern along with the Rietveld refinement considering the antisite disorder between the octahedral site atoms (i.e., V and Al). This is the best out of various fittings to the XRD data. In case of refinement using completely ordered Y-type structure, the observed intensity of the (111) peak is found to be less than the calculated one [see Fig. 1(c) 1(i)]. The match between the observed and the calculated intensities for other superlattice peaks is very good. The intensity of the XRD peaks is calculated from the square of the modulus of the structure factors for each (hkl) plane. The structure factor for a typical EQHA structure ($XX'YZ$) is given by

$$F_{hkl} = 4(f_Z + f_Y e^{i\pi(h+k+l)} + 2f_X e^{i\frac{\pi}{2}(h+k+l)} + f_{X'} e^{i\frac{3\pi}{2}(h+k+l)}), \tag{1}$$

where f_Z, f_Y, f_X, $f_{X'}$ are the atomic scattering factors for Z, Y, X, and X', respectively. For the superlattice peaks (111) and (200), the structure factor formula can be written as

$$F_{111} = 4[(f_Z - f_Y) - i(f_X - f_{X'})], \tag{2}$$

$$F_{200} = 4[(f_Y + f_Z) - (f_X + f_{X'})]. \tag{3}$$

As per equation (2), the reduction in the intensity of only the (111) peak indicates the mixing of the atoms between the

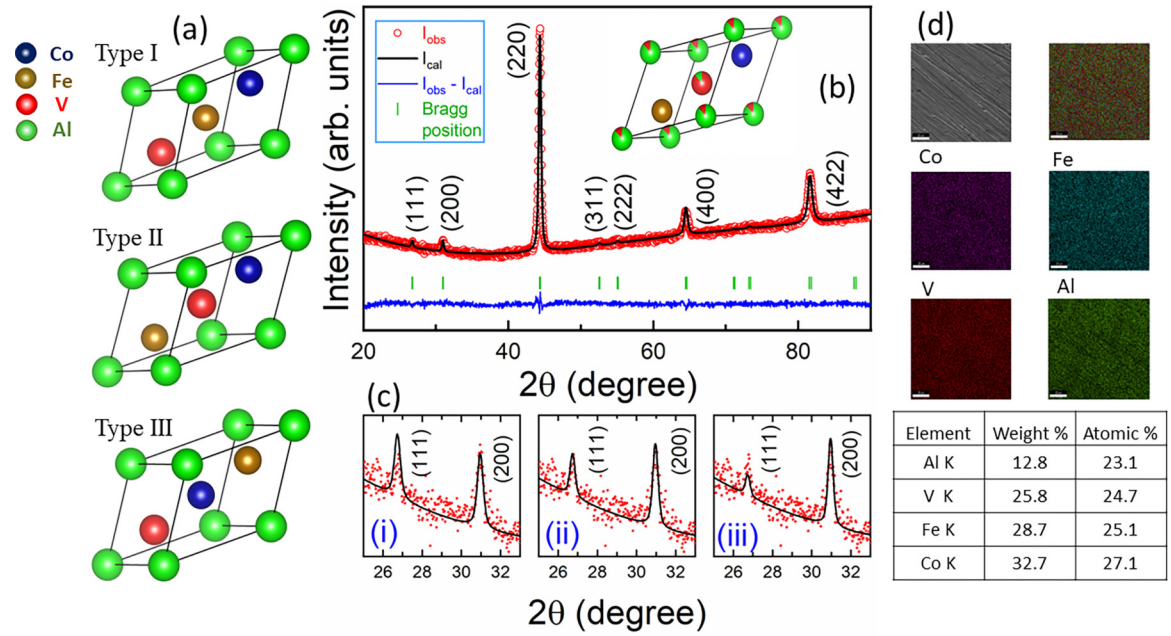

FIG. 1. For CoFeVAl: (a) The primitive unit cells of three possible nondegenerate ordered configurations. (b) Room temperature XRD pattern along with the Rietveld refinement considering B2-type antisite disorder between the octahedral sites V and Al only while keeping Fe and Co sites ordered. Inset shows the primitive cell of this B2 disordered structure. (c) The zoomed-in view of the refinement of two peaks (111) and (200) considering (i) completely ordered structure and (ii) 12.5% and (iii) 25% disordered structure between V and Al atoms. (d) Energy-dispersive x-ray spectroscopy results with elemental mapping and atomic compositions.

octahedral sites Z and Y or X and X' or both, which is known as the B2-type antisite disorder [22].

To determine the actual type of disorder, Rietveld refinement was carried out considering the mixing between the octahedral site atomic pairs V-Al and tetrahedral pairs Co-Fe together as well individually for various mixing compositions such as 12.5%, 25%, 37.5%, and 50%. The best fit is achieved while considering 12.5% disorder between V and Al only keeping Co and Fe sites ordered. The primitive cell of the B2 disordered structure is shown in the inset of Fig. 1(b). In Fig. 1(c) the fitting of the first two superlattice peaks (111) and (200) is shown for (i) completely ordered structure and (ii) 12.5% and (iii) 25% disordered structure between V and Al. The effect of antisite disorder on the intensity of the (111) peak is clearly visible from the aforementioned figures where the fitting gets better from zero disorder to 12.5% disorder and then gets worse for 25% disorder. The corresponding χ^2 value from the refinement is 1.05 for the completely ordered structure which reduces to 1.01 for the 12.5% B2 disordered structure.

Figure 1(d) shows the EDS results within an experimental uncertainty of ∼5%. The elemental mapping of constituent elements ensures the homogeneity of the sample including the absence of any kind of cluster formation. The table shows the atomic percentages of the as-prepared sample of CoFeVAl.

B. Magnetic properties

Figure 2(a) shows the variation of magnetization as a function of temperature (T) under the applied field $H = 100$ Oe. A sharp transition from the lower magnetization state to the higher magnetization state is observed at around 50 K for both ZFC and FCC data. The inset of this figure shows the variation of M with H for three different temperatures 2 K, 75 K, and 300 K. At 2 K, nearly saturating behavior of magnetization is observed with a value of 0.56 μ_B/f.u. at 70 kOe. At 75 K, the M-H curve is not at all saturating, suggesting the existence of some magnetization that keeps on increasing with the field. At 300 K, complete linear, paramagnetic behavior is observed in the M-H curve.

For Heusler systems, the maximum magnetic moment per formula unit can be calculated using the Slater-Pauling (S-P) rule. For EQHAs, the S-P rule is given by the equation [23,24]

$$M_t = N_V - 24, \tag{4}$$

where M_t is the total magnetic moment per formula unit and N_V is the total number of valance electrons in the alloy. According to the S-P rule, the expected magnetic moment in CoFeVAl is 1 μ_B/f.u. as N_V for CoFeVAl is 25.

Interestingly, the observed magnetization at 2 K is slightly less than that expected from the S-P rule. Any reduction of magnetization value from the S-P rule generally indicates the absence of complete spin polarization. Here for CoFeVAl, both the nearly saturating behavior in the M-H curve and the reduction in the magnetization value from the S-P rule indicate the presence of some antiparallel magnetic correlation in this system. The negligible coercivity throughout the temperature range (2 to 300 K) indicates the soft magnetic nature of CoFeVAl.

In order to find out the transition temperature we have used the Arrott plot [25], which is given by the relation

$$M^2 = (1/4b)H/M - (a/2b)\epsilon, \tag{5}$$

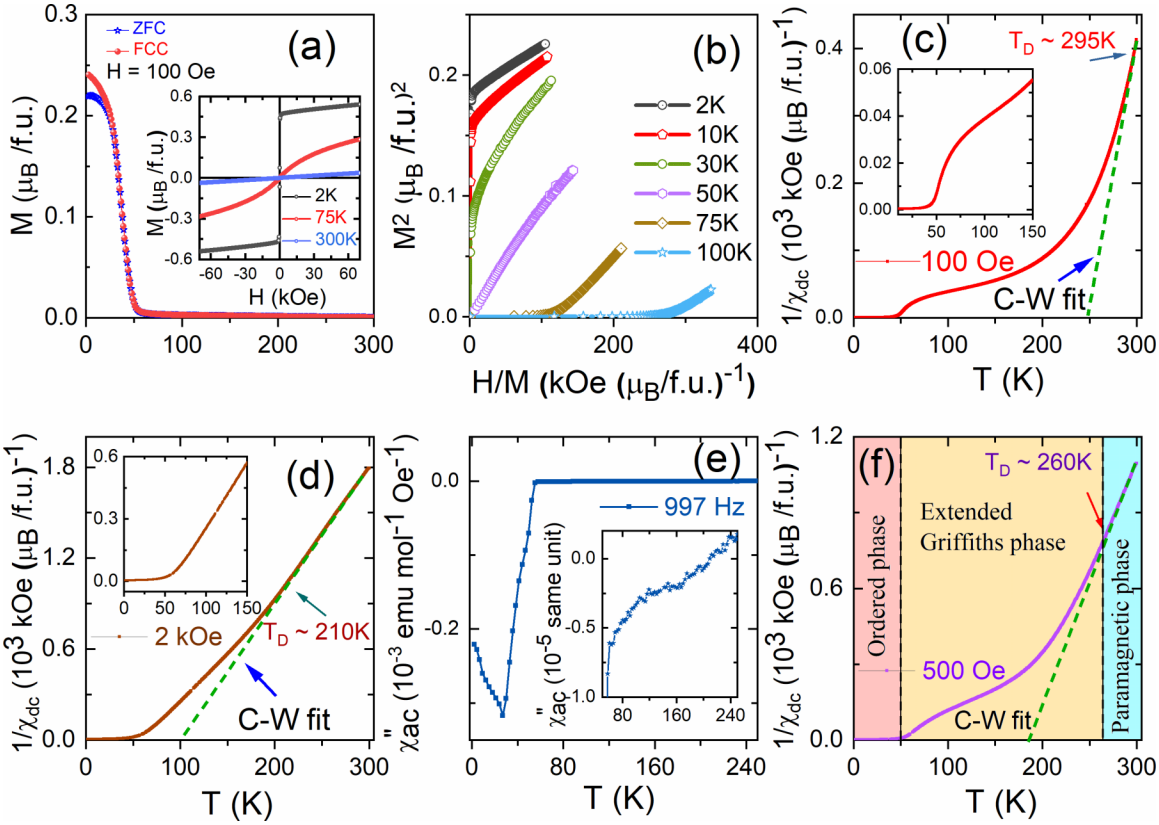

FIG. 2. For CoFeVAl: (a) Magnetization (M) vs temperature (T) for ZFC and FCC protocol under applied magnetic field $H = 100$ Oe. Inset shows the M vs H curves for temperatures 2, 75, and 300 K. (b) Arrott plots for different temperatures from 2 to 100 K. (c), (d) Inverse dc susceptibility vs T for 100 Oe and 2 kOe along with the Curie-Weiss (C-W) fitting. Insets of (c) and (d) show a zoomed-in view of the respective plots. (e) Imaginary part of the ac susceptibility vs T under 1 Oe bias field and 997 Hz excitation frequency. Inset shows a zoomed-in view of the same plot. (f) Magnetic phase diagram of the FCC data under 500 Oe which highlights the extended Griffiths phase region along with the C-W fitting.

where a and b are the material-dependant constants while the y intercept ϵ is given by the equation $\epsilon = (T - T_C)/T_C$, where T_C is the magnetic transition temperature. Figure 2(b) shows the Arrott plot for various temperatures from 2 K to 100 K. The positive/negative sign of ϵ indicates the magnetically disordered/ordered state. At the magnetic transition temperature, ϵ is zero. The linear fitting at higher fields in the M^2 vs H/M plot gives the positive intercepts for 2, 10, and 30 K. At 50 K, the y intercept is closest to zero among all the temperatures and for 75 K and 100 K the intercept is negative. Therefore, one can conclude that the transition to the magnetically ordered state occurs at/around 50 K ($T_C = 50$ K) and there is no spontaneous magnetization present in the system above this temperature. This observation is in line with the M-T curve shown in Fig. 2(a).

To further investigate the magnetic phenomena, we have studied the dc magnetic susceptibility as a function of temperature in the FCC protocol under magnetic fields 100 Oe, 2 kOe, and 500 Oe; see Figs. 2(c), 2(d) and 2(f). In the paramagnetic regime, we have fitted the inverse of the dc susceptibility data (χ_{dc}^{-1}) using the Curie-Weiss (C-W) formula which is given by $1/\chi = (T - \theta_{CW})/C$, where C is the Curie constant and θ_{CW} is the Curie-Weiss temperature. For all the three fields, χ_{dc}^{-1} deviates from the Curie-Weiss behavior when the sample is cooled from room temperature and we mark the deviation temperatures as T_D in the respective plots. The values of T_D are 295 K, 260 K, and 210 K for the applied fields 100 Oe, 500 Oe, and 2 kOe, respectively, which implies that with increasing fields, T_D shifts toward lower temperatures. For the FCC data under 100 Oe, from 295 K, χ_{dc}^{-1} decreases continuously with decrease in temperature until 50 K where it takes a sharp downturn and becomes zero indicating the magnetically ordered state. The downturn that started just above 50 K becomes less sharp for 500 Oe data and completely vanishes in 2 kOe. In the inset of Figs. 2(c) and 2(d), a zoomed-in view of the respective plots is shown where the downturn of χ_{dc}^{-1} is clearly visible.

The deviation from the C-W behavior below T_D indicates the existence of some net magnetization above the magnetic ordering temperature, which may arise out of nucleation or local alignment of small ferromagnetic clusters [9]. This type of nucleation becomes stronger as the temperature decreases, and near the magnetic transition temperature, it causes a sharp downturn in χ_{dc}^{-1} making it negligibly small or zero. The shifting of T_D toward lower temperature with increasing field indicates that the paramagnetic contribution from the sample, with the increasing field, increases and overshadows the contribution from the magnetic clusters [9,26,27]. The

paramagnetic contribution also masks out the downturn immediately above the magnetic transition temperature as it becomes less sharp with the increase of magnetic fields [26]. The nucleation of magnetic clusters above the magnetic ordered state is often observed in diluted ferromagnetic alloys [27–30] and more recently also in some Heusler alloys [9,31,32], where it is attributed to the Griffiths phase–like behavior. But in our system, the magnetic cluster formation is different from the earlier studies as it exists for a much larger temperature range, but several features including the variation with the magnetic field are quite similar to those of the earlier reports.

We have also studied the T dependence of ac magnetic susceptibility (χ_{ac}) in the presence of 1 Oe dc bias field and an ac excitation frequency of 997 Hz to further explore the unusual magnetic behavior above the transition temperature. Figure 2(f) shows the imaginary part (χ''_{ac}) of the ac magnetic susceptibility as a function of temperature. The nonzero value of χ''_{ac} indicates the existence of magnetization in the sample [26]. Here, when the sample is cooled from 300 K, χ''_{ac} takes a sharp downward shoot near 50 K, which indicates the magnetic transition temperature. The inset of Fig. 2(f) shows a zoomed-in view of χ''_{ac} vs T, which clearly indicates a nonzero value throughout the temperature range and this value (although small in magnitude) keeps on increasing as the sample is cooled. This kind of behavior of χ''_{ac} assures the existence of a small net magnetization above the magnetically ordered state which increases with the decrease in temperature.

The Griffiths phase is identified as the magnetic region that exists between the clean (magnetically ordered) and dirty (magnetically disordered/paramagnetic) phases. The persistence of small net magnetization above magnetic ordering temperature and its dependence on the applied field are the main indications of the presence of the Griffiths-like phase. Such a phase is mainly observed under an externally applied field where the logarithmic dependence of the susceptibility inverse (χ^{-1}) in the temperature scale shows a weakening with increasing field. In our system, CoFeVAl, we have clearly observed the above features confirming the presence of the Griffiths-like phase. In most reported candidate systems such as diluted ferromagnetic manganites [33,34], cobaltites [35,36], intermetallics [37,38], and Heusler alloys [9,31,39], the Griffiths phase is found to exist in a very narrow temperature range and is attributed to the quenched disorder present in the system. In contrast, for CoFeVAl, this phase is found to exist for an unusually large temperature range with a characteristic nonlinear temperature dependence of magnetization. In Fig. 2(f), the magnetic phase diagram is shown for the FCC data under 500 Oe, where the co-existing of three different magnetic phases in three different region in the temperature scale is highlighted. Such a temperature dependence not only distinguishes this system from the other reported systems hosting this phase, but also indicates the presence of some magnetic correlations among the magnetic clusters. The existence of the Griffiths phase for such a large temperature range encourages us to parse it as extended Griffiths phase. As shown below, our transport measurements also give enough hints supporting the existence of the Griffiths-like phase in CoFeVAl.

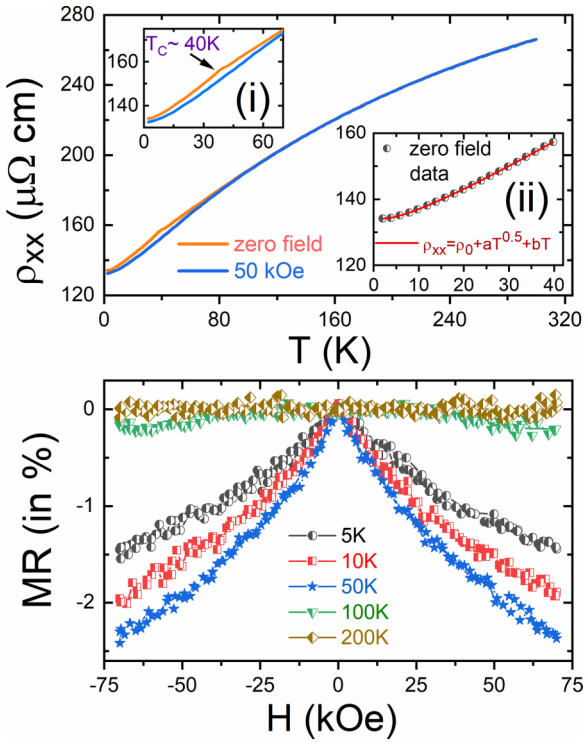

FIG. 3. For CoFeVAl: (a) Longitudinal resistivity (ρ_{xx}) vs temperature (T) for zero and 50 kOe applied field. Inset (i): Zoomed-in view of ρ_{xx} vs T to highlight the hump near 40 K. Inset (ii): Low-temperature fitting of the zero-field ρ_{xx} data. (b) Magnetoresistance (MR) vs applied field (H) for various temperatures.

C. Transport properties

1. Resistivity

Figure 3(a) shows the temperature variation of longitudinal resistivity (ρ_{xx}) at 0 and 50 kOe field. The monotonic increase of ρ_{xx} from ∼130 μΩ cm to ∼270 μΩ cm in the T range of 2 to 300 K indicates the metallic nature of CoFeVAl. While cooling down from 300 K, a very small deviation in the ρ_{xx} is observed below 80 K between the zero-field data and 50 kOe data. This small deviation is clearly visible in the inset (i) of Fig. 3(a). ρ_{xx} reduces to a lower value in the presence of magnetic field, which can be attributed to the suppression of spin disorder scattering by the applied field [40]. A shallow hump-like feature is observed at around 40 K in the zero-field data as compared to the 50 kOe data. This may arise due to the magnetic transition at/around this temperature [22].

To analyze the extent of various scattering contributions to ρ_{xx} in the low-temperature range, we have fitted the ρ_{xx} data up to 40 K considering several scattering mechanisms such as electron-electron (e-e) elastic scattering, electron-phonon (e-p) scattering, and electron-magnon (e-m) scattering [40]. The fitting is tried considering various combinations of these contributions and the best fit is obtained via the following relation,

$$\rho_{xx} = \rho_0 + aT^{0.5} + bT, \tag{6}$$

where ρ_0 represents the temperature-independent residual resistivity. The $T^{0.5}$ term represents the contribution from

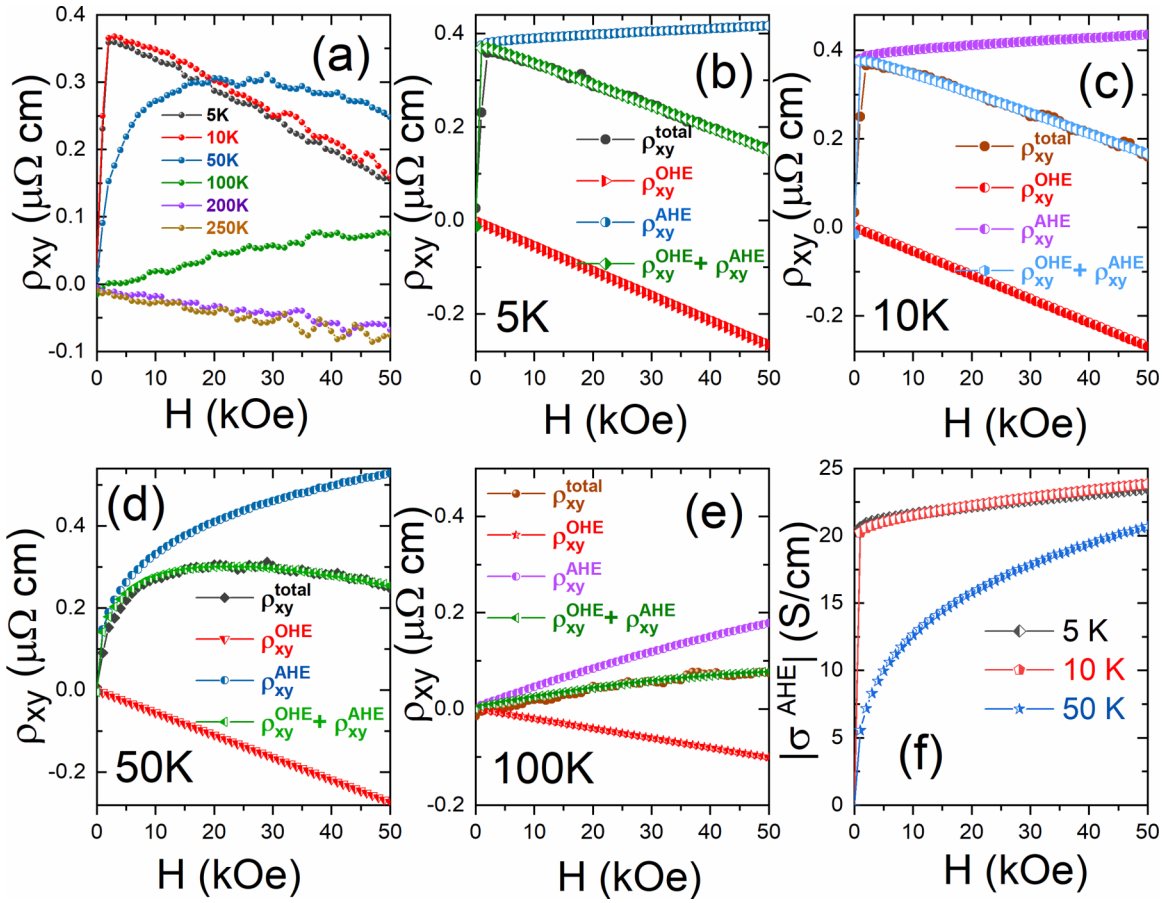

FIG. 4. For CoFeVAl: (a) Hall resistivity ρ_{xy} vs H for various temperatures up to 250 K. ρ_{xy} vs H along with separated ordinary (ρ_{xy}^{OHE}) and anomalous (ρ_{xy}^{AHE}) Hall contributions for (b) 5 K, (c) 10 K, (d) 50 K, and (e) 100 K. (f) Intrinsic anomalous Hall conductivity ($\sigma_{\mathrm{int}}^{\mathrm{AHE}}$) vs H for 5, 10, and 50 K.

e-e elastic scattering, while the linear term (T) represents the e-p scattering. Inset (ii) of Fig. 3(a) shows the low-temperature fitting of ρ_{xx} data. The fitting parameters are residual resistivity, $\rho_0 = (136.1 \pm 0.1)\ \mu\Omega$ cm, $a = -(2.81 \pm 0.06)\ \mu\Omega$ cm $K^{-0.5}$, and $b = (0.978 \pm 0.008)\ \mu\Omega$ cm K^{-1}. The negative sign of the e-e contribution is in line with the other reported similar Heusler alloy, CoFeVSb [12,41]. We have also fitted the data including the e-m scattering which goes as T^2 in the ρ_{xx} expression and have found an unrealistically small value of the corresponding coefficient. This confirms that the e-m scattering is negligibly small and hence gets masked out in comparison to other dominant scattering. This is an indirect indication of the nearly half-metallic behavior in CoFeVAl.

2. Magnetoresistance

Figure 3(b) shows the magnetoresistance of CoFeVAl as a function of field at several temperatures, where MR is defined by $\mathrm{MR}(H) = [\rho_{xx}(H) - \rho_{xx}(0)]/\rho_{xx}(0) \times 100\%$. A negative MR is observed for temperatures up to 50 K, beyond which the magnitude of MR is negligibly small. Negative MR is usually observed in ferromagnetic materials mostly due to the suppression of spin disorder scattering by the application of magnetic field [40]. Here 1.5% MR is observed for 5 K and it increases to 2.5% at 50 K. As the sample is cooled below the magnetic transition temperature, the spin disorder decreases, resulting in a decrease in the MR value. The effect of unusual magnetic phase above 50 K is also reflected in the MR data at 100 K. At high fields such as 50 kOe, the masking of magnetic clusters by the paramagnetic contribution causes the reduction of small e-m scattering, resulting in almost negligible MR. The symmetric feature of MR with the change of magnetic field direction for all the temperatures ensures the soft magnetic nature of CoFeVAl.

3. Hall resistivity

In order to investigate the response of transverse resistivity to the applied magnetic field, we have studied the Hall resistivity of CoFeVAl. The raw Hall data are antisymmetrized by using the relation $\rho_{xy}^{\mathrm{Hall}} = [\rho_{xy}^{\mathrm{raw}}(H) - \rho_{xy}^{\mathrm{raw}}(-H)]/2$ in order to subtract any MR contribution in the Hall data [42]. The resulting Hall resistivity vs magnetic field for various temperatures up to 250 K is shown in Fig. 4(a). For 5 K and 10 K, the Hall resistivity shows a steep increase at very low field and then decreases as the field increases further. The steep increase is less for 50 K, and so is the decrement at the higher fields. For 100 K, an unusual behavior is observed. The usual reduction at higher fields is absent even up to 50 kOe; rather a linear increase with the field is observed throughout the field range. For 200 and 250 K, a negative linear Hall response is

observed. In general, the Hall resistivity is dominated by the ordinary Hall effect (OHE) at higher fields. But in the present case, the significant difference in the Hall resistivity at higher fields among the different temperatures indicates the presence of another significant contribution even at higher fields. To investigate this further, we have separated out different contributions by using the relation

$$\rho_{xy}^{\text{total}} = \rho_{xy}^{\text{OHE}} + \rho_{xy}^{\text{AHE}} = R_0 H + R_S M = R_0 H + b\rho_{xx}^2 M, \tag{7}$$

where ρ_{xy}^{OHE} and ρ_{xy}^{AHE} are the ordinary and anomalous Hall contributions to the total Hall resistivity; R_0 and R_S are the ordinary and anomalous Hall coefficients, respectively. R_S is further simplified using the relation $R_S = b\rho_{xx}^2$, where b is the coefficient of the intrinsic anomalous Hall effect. Here, we have considered only the intrinsic contribution to AHE because the order of longitudinal conductivity ($\sigma_{xx} \sim 10^3$ S/cm) suggests the possible absence of skew scattering contributions [43] and for ferromagnetic metals the extrinsic side jump contribution to anomalous Hall conductivity is negligibly small [44,45]. Using equation (7) and the intercept and slope of the $\rho_{xy}^{\text{total}}/H$ vs $\rho_{xx}^2 M/H$ plot, we first found R_0 and R_S [46] and then calculated ρ_{xy}^{OHE} and ρ_{xy}^{AHE}. In Figs. 4(b)–4(e), different contributions to ρ_{xy}^{total} are shown for temperatures 5, 10, 50, and 100 K. For 5 and 10 K, the ρ_{xy}^{AHE} is nearly saturated at around 0.4 μΩ cm. But near the magnetic transition at 50 K, the nonsaturating behavior is observed in ρ_{xy}^{AHE} with a value of around 0.5 μΩ cm at 50 kOe. For 100 K data, it is clear that AHE still persists, possibly attributable to the magnetic clusters present in the system at this temperature. To further evaluate the actual contribution of intrinsic AHE, we have calculated intrinsic anomalous Hall conductivity ($\sigma_{\text{int}}^{\text{AHE}}$) using the relation [9] $|\sigma_{\text{int}}^{\text{AHE}}| \approx \rho_{xy}^{\text{AHE}}/\rho_{xx}^2$. Figure 4(f) shows the variation of $|\sigma_{\text{int}}^{\text{AHE}}|$ with magnetic field at different T. For 5 and 10 K, $\sigma_{\text{int}}^{\text{AHE}}$ shows a nearly saturating behavior and attains a value of around 24 S/cm at 50 kOe. A nonsaturating behavior of $\sigma_{\text{int}}^{\text{AHE}}$ is observed at 50 K with a magnitude of around 21 S/cm at 50 kOe. Since the intrinsic contribution of the AHE directly correlates with the spontaneous magnetization, the behavior of AHE with applied field at different temperatures reflects the $M(H)$ and the reduction in the value at 50 K corresponds to the reduction in spontaneous magnetization near the magnetic transition temperature.

From the OHE contribution, we have obtained $R_0 = -(5.303 \pm 0.113) \times 10^{-3}$ μΩ cm (kOe)$^{-1}$ and hence the intrinsic carrier concentration $n = 1.18 \times 10^{22}$ cm^{-3} at 5 K. This negative value of R_0 is found to appear for all temperatures, indicating the electron-mediated conduction in CoFeVAl. The order of magnitude and almost constant nature of n with temperature reconfirms the metallic behavior of CoFeVAl.

D. Theoretical results

Ab initio calculations are performed for the three possible nondegenerate atomic configurations (see Sec. III A) of CoFeVAl. The type II configuration is found to be lowest in energy with the optimized lattice parameter $a_0 = 5.72$ Å, which agrees with an earlier report [47]. The simulated lattice parameter is in good agreement with the experimentally observed one (5.78 Å). To identify the actual magnetic ground state, we have relaxed the structure considering various magnetic orderings including ferromagnetic, antiferromagnetic, and ferrimagnetic configurations for all three atomic arrangements. A type II structure with a ferrimagnetic ordering is found to be the ground state (with V atoms aligned antiparallel to Co and Fe). Table I shows the simulated results for theoretically optimized lattice parameters a_0, atom projected on-site magnetic moments, total magnetic moments, and the formation energies for the three possible configurations. Figure 5 (top panel) shows the spin-polarized density of states (DOS) and band structure of CoFeVAl in the fully ordered type II configuration. In the completely ordered type II structure, the total magnetic moment is mostly contributed by Co and Fe, being ferromagnetically coupled to each other, whereas V has a very small antiparallel moment. This confirms a nearly ferromagnetic-like ground state which corroborates well with our experimental observation. From the DOS, the spin polarization is calculated to be 86%, which suggests the nearly half-metallic behavior of CoFeVAl. The only electron pocket in the spin-down band, which causes

TABLE I. For CoFeVAl: Relaxed lattice parameter (a_0), atom-projected on-site magnetic moments (in μ_B), total magnetic moments (in μ_B), and formation energies E_f for type I, II, and III configurations in the ordered state and B2 disordered phase. The atom-projected moments in the disordered case are averaged moments.

Type	a_0 (Å)	m^{Co}	m^{Fe}	m^{V}	m^{tot}	E_f (eV/f.u.)
I	5.83	1.003	2.412	−1.168	2.238	−0.68
II	5.72	0.616	0.466	−0.040	1.032	−1.56
III	5.82	1.405	2.100	−0.384	3.115	−0.26
Disorder	5.73	0.601	0.402	−0.050	0.951	−1.50

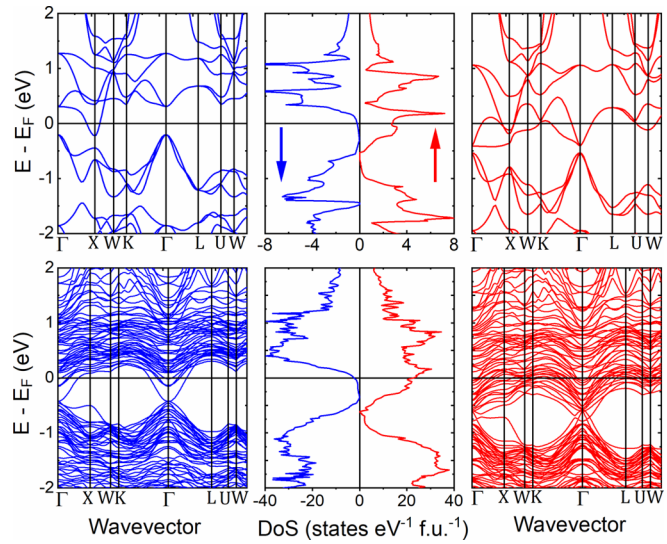

FIG. 5. For CoFeVAl: Spin-polarized band structure and density of states (DOS) for the (top) completely ordered structure and (bottom) B2 disordered structure.

a small reduction from the complete spin polarization, is originated from the V-3*d* orbitals.

Keeping in mind the experimental findings for the antisite disorder, we have also simulated the electronic structure of B2 disordered CoFeVAl (with 12.5% antisite disorder between V and Al). This is done by generating an SQS structure (32 atoms) and relaxing it completely. The structural, atom projected (average), and total magnetic moments and the formation energy for this structure are shown in Table I. The lattice parameter almost remains the same in the disordered state, whereas some subtle changes have been observed in the magnetic structure. In the disordered state, magnetic moments at some of the V sites are ferromagnetically coupled while some retain antiferromagnetic coupling as in the ordered case. Since V sites carry very small moment, the average moment of the V sites remains almost unaltered. The V atom that actually occupies the Al site (because of the disorder) carries very small positive moment whereas Al itself carries negligibly small moments. Moreover, because of the changes in the local environment due to antisite disorder, the average magnetic moment at Fe sites reduces as compared to the ordered state. This is mainly responsible for a little reduction in the total moment as compared to the ordered state value, i.e., 0.95 μ_B/f.u. We have calculated the spin polarization for the disordered phase which is almost the same (∼83%) as that of the ordered state. Figure 5 (bottom panel) displays the spin-polarized DOS and band structure for the disordered structure of CoFeVAl. Due to the reduction in the symmetry mediated by the antisite disorder, the small electron pocket gets shifted to the Γ point but its origin remains the same. Since the spin polarization value does not change much, we conclude that nearly half-metallic behavior remains intact even in the presence of disorder.

The experimentally observed value of saturation magnetization is still less than what we have obtained from simulation. To unravel the origin behind this, we have performed self-consistent calculations by using a few representative Hubbard parameters U applied individually on Co, Fe, V and also including a few combinations of them. The values of U are taken in the range of 3–6 eV. These calculations did not reduce the total magnetic moment much (lowest value achieved is 0.9 μ_B/f.u.). As such, the experimentally observed (reduced) value of saturation magnetization might originate from the nonsaturating or nearly saturating behavior of magnetization in CoFeVAl.

IV. SUMMARY AND CONCLUSION

To summarize, we report a combined theoretical and experimental study of the electronic, magnetic, and transport properties of the quaternary Heusler alloy CoFeVAl. It shows a magnetic phase above the magnetic transition temperature, namely the extended Griffiths-like phase, as revealed by the unusual behavior of dc and ac susceptibility. Interestingly the Curie temperature seen in the sister compound CoFeVSb decreases considerably on replacing Sb by Al. Similarly, the spin valve feature seen in the former is completely absent in the latter. CoFeVAl crystallizes in a cubic structure (space group No. 216) with B2-type disorder (12.5% antisite disorder between V and Al), as confirmed by XRD measurement. It shows a nearly half-metallic ferromagnetic behavior, with reasonably high spin polarization (∼86%). *Ab initio* calculations for ordered CoFeVAl confirm a very small moment on vanadium sites aligned antiparallel to Co and Fe, giving rise to a net magnetization of 0.9 μ_B/f.u. The nearly half-metallic ferromagnetism remains unaltered even in the B2 disordered phase. Similarly to CoFeVSb, the total magnetic moment of CoFeVAl is majorly contributed by Co and Fe. In CoFeVSb, the ferromagnetic/antiferromagnetic interface that gave rise to the spin valve feature was developed because of the disorder between Co and Fe sites. In CoFeVAl, the main magnetic elements Co and Fe are not involved in the antisite disorder, which prevents the formation of any strong antiferromagnetic layer resulting in the absence of the spin valve feature. Rather the antisite disorder is found between the other two atoms V and Al which is possibly the reason behind the extended Griffiths phase behavior, which is quite an unusual behavior in this family of alloys.

ACKNOWLEDGMENTS

B.B. acknowledges CSIR, India, for the financial support to carry out this project. The authors acknowledge Aniruddha Patil for the XRD measurements in the High Resolution X-Ray Diffractometer, Department of Physics, IIT Bombay. K.G.S. thanks DST, Government of India, for Sponsored Project No. DST/INT/RUS/RSF/P-47/2021 (G).

[1] K. Elphick, W. Frost, M. Samiepour, T. Kubota, K. Takanashi, H. Sukegawa, S. Mitani, and A. Hirohata, Sci. Technol. Adv. Mater. **22**, 235 (2021).
[2] L. Bainsla and K. G. Suresh, Appl. Phys. Rev. **3**, 031101 (2016).
[3] R. A. de Groot, F. M. Mueller, P. G. van Engen, and K. H. J. Buschow, Phys. Rev. Lett. **50**, 2024 (1983).
[4] C. Felser, G. H. Fecher, and B. Balke, Angew. Chem. Int. Ed. **46**, 668 (2007).
[5] V. Alijani, J. Winterlik, G. H. Fecher, S. S. Naghavi, and C. Felser, Phys. Rev. B **83**, 184428 (2011).
[6] L. Bainsla, A. Mallick, M. M. Raja, A. I. Nigam, B. S. S. Ch. Varaprasad, Y. K. Takahashi, A. Alam, K. G. Suresh, and K. Hono, Phys. Rev. B **91**, 104408 (2015).
[7] J. Nag, D. Rani, J. Kangsabanik, D. Singh, R. Venkatesh, P. D. Babu, K. G. Suresh, and A. Alam, Phys. Rev. B **104**, 134406 (2021).
[8] Y. Venkateswara, S. S. Samatham, P. D. Babu, K. G. Suresh, and A. Alam, Phys. Rev. B **100**, 180404(R) (2019).
[9] J. Nag, P. C. Sreeparvathy, R. Venkatesh, P. D. Babu, K. G. Suresh, and A. Alam, Phys. Rev. Appl. **19**, 044071 (2023).
[10] D. Rani, J. Kangsabanik, K. G. Suresh, N. Patra, D. Bhattacharyya, S. N. Jha, and A. Alam, Phys. Rev. Appl. **10**, 054022 (2018).
[11] S. Paul, A. Kundu, B. Sanyal, and S. Ghosh, J. Appl. Phys. **116**, 133903 (2014).

[12] J. Nag, D. Rani, D. Singh, R. Venkatesh, B. Sahni, A. K. Yadav, S. N. Jha, D. Bhattacharyya, P. B. Babu, K. G. Suresh, and A. Alam, Phys. Rev. B **105**, 144409 (2022).
[13] J. Rodríguez-Carvajal, Phys. B: Condens. Matter **192**, 55 (1993).
[14] P. Hohenberg and W. Kohn, Phys. Rev. **136**, B864 (1964).
[15] G. Kresse and J. Furthmüller, Phys. Rev. B **54**, 11169 (1996).
[16] G. Kresse and J. Furthmüller, Comput. Mater. Sci. **6**, 15 (1996).
[17] G. Kresse and J. Hafner, Phys. Rev. B **47**, 558(R) (1993).
[18] G. Kresse and D. Joubert, Phys. Rev. B **59**, 1758 (1999).
[19] J. P. Perdew, K. Burke, and M. Ernzerhof, Phys. Rev. Lett. **77**, 3865 (1996).
[20] A. Zunger, S.-H. Wei, L. G. Ferreira, and J. E. Bernard, Phys. Rev. Lett. **65**, 353 (1990).
[21] A. van de Walle, P. Tiwary, M. de Jong, D. L. Olmsted, M. Asta, A. Dick, D. Shin, Y. Wang, L.-Q. Chen, and Z.-K. Liu, Calphad **42**, 13 (2013).
[22] S. Chatterjee, S. Chatterjee, S. Giri, and S. Majumdar, J. Phys.: Condens. Matter **34**, 013001 (2022).
[23] N. Zheng and Y. Jin, J. Magn. Magn. Mater. **324**, 3099 (2012).
[24] K. Özdoğan, E. Şaşıoğlu, and I. Galanakis, J. Appl. Phys. **113**, 193903 (2013).
[25] A. Arrott, Phys. Rev. **108**, 1394 (1957).
[26] A. Karmakar, S. Majumdar, S. Kundu, T. K. Nath, and S. Giri, J. Phys.: Condens. Matter **25**, 066006 (2013).
[27] W. Jiang, X. Zhou, and G. Williams, Europhys. Lett. **84**, 47009 (2008).
[28] A. K. Pramanik and A. Banerjee, Phys. Rev. B **81**, 024431 (2010).
[29] N. Adeela, U. Khan, S. Naz, M. Iqbal, M. Irfan, and Y. Cheng, Appl. Surf. Sci. **422**, 184 (2017).
[30] P. T. Phong, L. T. T. Ngan, N. V. Dang, L. H. Nguyen, P. H. Nam, D. M. Thuy, N. D. Tuan, L. V. Bau, and I. J. Lee, J. Magn. Magn. Mater. **449**, 558 (2018).
[31] S. Chatterjee, S. Giri, S. Majumdar, P. Dutta, P. Singha, and A. Banerjee, J. Phys.: Condens. Matter **34**, 295803 (2022).
[32] A. Ślebarski, J. Goraus, and M. Fijałkowski, Phys. Rev. B **84**, 075154 (2011).
[33] S. Saha, A. Dutta, S. Gupta, S. Bandyopadhyay, and I. Das, Phys. Rev. B **105**, 214407 (2022).
[34] G. Singh, A. Gaur, P. Bisht, and R. N. Mahato, J. Magn. Magn. Mater. **591**, 171731 (2024).
[35] I. Fita, I. O. Troyanchuk, T. Zajarniuk, P. Iwanowski, A. Wisniewski, and R. Puzniak, Phys. Rev. B **98**, 214445 (2018).
[36] Y. Shimada, S. Miyasaka, R. Kumai, and Y. Tokura, Phys. Rev. B **73**, 134424 (2006).
[37] K. Ghosh, C. Mazumdar, R. Ranganathan, S. Mukherjee, and M. De Raychaudhury, Phys. Rev. B **98**, 184419 (2018).
[38] S. Ubaid-Kassis, T. Vojta, and A. Schroeder, Phys. Rev. Lett. **104**, 066402 (2010).
[39] S. Chakraborty, S. Gupta, and C. Mazumdar, J. Alloys Compd. **976**, 173215 (2024).
[40] D. Bombor, C. G. F. Blum, O. Volkonskiy, S. Rodan, S. Wurmehl, C. Hess, and B. Büchner, Phys. Rev. Lett. **110**, 066601 (2013).
[41] A. Chanda, J. Nag, A. Alam, K. G. Suresh, M.-H. Phan, and H. Srikanth, Phys. Rev. B **107**, L220403 (2023).
[42] G. K. Shukla, J. Sau, N. Shahi, A. K. Singh, M. Kumar, and S. Singh, Phys. Rev. B **104**, 195108 (2021).
[43] N. Nagaosa, J. Sinova, S. Onoda, A. H. MacDonald, and N. P. Ong, Rev. Mod. Phys. **82**, 1539 (2010).
[44] S. Roy, R. Singha, A. Ghosh, A. Pariari, and P. Mandal, Phys. Rev. B **102**, 085147 (2020).
[45] Y. Liu, H. Tan, Z. Hu, B. Yan, and C. Petrovic, Phys. Rev. B **103**, 045106 (2021).
[46] A. Singh, V. K. Gangwar, P. Shahi, D. Pal, R. Singh, S. Kumar, S. Singh, S. K. Gupta, S. Kumar, J. Cheng, and S. Chatterjee, Appl. Phys. Lett. **117**, 092403 (2020).
[47] L. Xiong, L. Yi, and G. Y. Gao, J. Magn. Magn. Mater. **360**, 98 (2014).